IEEE Access
Multidisciplinary | Rapid Review | Open Access Journal

Received June 22, 2018, accepted July 28, 2018, date of publication August 3, 2018, date of current version September 5, 2018.

Digital Object Identifier 10.1109/ACCESS.2018.2863024

Analysis of Sandstone Pore Space Fluid Saturation and Mineralogy Variation via Application of Monostatic K-Band Frequency Modulated Continuous Wave Radar

JAMIE BLANCHE[1], (Student Member, IEEE), DAVID FLYNN[1], (Member, IEEE), HELEN LEWIS[2], GARY D. COUPLES[2], JIM BUCKMAN[2], CHRIS BAILEY[3], (Senior Member, IEEE), AND TIMOTHY TILFORD[3]

[1]Smart Systems Group, Heriot-Watt University, Edinburgh EH14 4AS, U.K.
[2]Institute of Petroleum Engineering, Heriot-Watt University, Edinburgh EH14 4AS, U.K.
[3]Department of Mathematical Sciences, University of Greenwich, London SE10 9LS, U.K.

Corresponding author: Jamie Blanche (jrb31@hw.ac.uk)

This work was supported by the Energy Technology Partnership (ETP) and Maersk/Total S.A. under Grant ETP 87/B12S10307.

ABSTRACT In this paper, we present the preliminary findings from a world-first investigation into monostatic frequency modulated continuous wave (FMCW) radar analysis of porous sandstones and their fluid content. FMCW results, within 24 to 25.5 GHz, provide insights into the rock/pore system as well as into mineral and liquid distributions, both crucial for the quantitative representation of the fluid-rock system for subsequent assessment of the sandstones. Sandstone samples, here characterised using known techniques of energy dispersive x-ray analysis, gaseous secondary electron (GSE) and backscattered electron (BSE) imaging are: Darney, Lazonby, Locharbriggs, and Red St. Bees sandstones, with FMCW results showing that, in the K-Band, the calculated values for relative permittivity, utilising free-space radiation reflection data, give results that are consistent with, and have the potential to predict, the known rock elemental constituents, where each sandstone has different distributions of the dominant quartz and subsidiary other minerals and of grain size and shape distributions. The experimental results support the sensitivity of this sensing modality to variances in rock properties in typical sandstones with complex relative permittivity, ε_r^*, values for room-dry sandstones ranging from 5.76 to 6.76 and from 12.96 to 48.3 for partially saturated sandstones, with the highest values indicating high relative permittivity mineral inclusion and/or grain angularity. FMCW provides similar results, over slightly larger volumes, to those produced by the current resource-intensive methodologies, but much more easily and cheaply.

INDEX TERMS Geologic measurements, microwave propagation, non-destructive testing, permittivity, radar applications, radar measurements.

I. INTRODUCTION

Reservoir management is used throughout the life cycle of oil and gas fields and is integral to safe and efficient recovery and storage of resources. An essential tool of reservoir management is a mass–fluid flow simulation, within which different production scenarios can be trialled and their practical, economic and environmental consequences investigated. Such simulations are critically dependent on the arrangement and properties of the *in situ* geomaterials, their pore network connectivity, fluid content and the deformational responses of those materials to natural subsurface and operationally-induced conditions [1]. The same concepts apply to sites investigated for carbon capture and storage (CCS) suitability [2]–[4] and also provide a means of mitigating risk when sites are exposed to loading events [5]. The research within this paper is novel as FMCW for the detection of critical geomaterial properties represents a new microwave sensing modality with seminal results of monostatic testing presented and supported by extensive experimental analysis. The current role of microwave sensing in the oil and gas sector is focused on petroleum system seal integrity via permittivity measurement during airborne

deployment, measurement of offshore oil spillage area via orbital remote sensing, and infrastructure health monitoring via embedded structural sensing [6]–[8]. Relative permittivity measurements obtained via microwave sensing form a key part of industrial hardware employed to interrogate the bore radius, however microwave sensing in this field has remained within a frequency spectrum from hundreds of megahertz to 1 GHz [9]. These applications of microwave sensing highlight the increasing usefulness of this sensing modality to the hydrocarbon sector as a means of collecting key data, both for application to production management and to resource/asset modelling.

Highly developed seismic acquisition and processing technology, together with wire-line sensors for use in the wellbore environment, are used to generate geomodels of the distribution of the different rock types in the subsurface and to estimate their petrophysical properties, occasionally achieving detailed predictions. The resolution of a seismic signal, a function of reflected acoustic waves due to changes in geomaterial acoustic impedance, is restricted to one quarter of the wavelength of the propagating wave, often equating to a minimum effective resolution scale in the order of tens of metres. However, data analysis and interpretation techniques employed by geoscientists and reservoir engineers can infer the presence of fine stratal units via the application of wavelet models [10]. These methods can be ambiguous and contain large uncertainties. However even the best seismic-based techniques are insufficient to provide data at the sub-millimetre scale, the scale required to resolve grain-pore structures, The purpose of the work reported here is to extend the range of real-time non-invasive and non-destructive tool types and measurement techniques down to the millimetre scale via the novel use of advanced radar electronics [11]. Advances in sensor performance at the millimetre to sub-millimetre scale represent a significant increase in geomaterial property quantification via an improved understanding of micro-interactions. At this preliminary stage, these techniques are envisaged for laboratory use where the sample is accessible.

Section II provides background information into FMCW with section II/A outlining FMCW theory, section II/B will discuss the application of FMCW to dielectric media. Section III outlines work conducted by research groups using FMCW for a variety of applications; section III/A focusing on FMCW used for corrosion under insulation detection, section III/B reviews FMCW use for snow thickness studies and section III/C outlines previous work by the authors in the novel use of FMCW for the analysis of geomaterials. Section IV reviews the application of dielectric theory to geomaterials and resulting models with section IV/A/1 discussing parallel field models, section IV/A/2 discusses series field models and layering Section IV/A/3 outlines the derivation and application of the complex refractive index method. Section V presents equipment and geomaterial characterisation, with section V/A outlining antenna characterisation work. Section V/B provides an analysis of geomaterial constituents and fabric. Section V/C outines the experimental setup and data acquisition procedure. Section VI presents the results acquired from this study, with section VI/A discussing the application of the layering models. Section VII outlines a discussion of the results. Section VIII concludes.

II. RADAR AND DIELECTRIC THEORY

A. FREQUENCY MODULATED CONTINUOUS WAVE GENERAL THEORY

FMCW represents a continuous wave, instead of the more commonly used pulsed wave radar. Frequency modulation gives a frequency shift over time to create a saw-tooth or triangular frequency output. A difference in frequency between the transmitted and received signals is determined by mixing output and input waveforms to give a new, low frequency signal, which can be analysed to calculate the distance and velocity of an object. The difference in frequency observed between received and output signals is calculated and transmitted to a data logger as an Intermediate Frequency (IF) signal of frequency Δf [12]. An overview of the determination of the IF signal of frequency Δf is as follows:

$$f_{\mathrm{RFOUT}} = f_{\mathrm{RFO}} + k_f * t, \quad where\ 0 \leq t \leq T \tag{1}$$

f_{RFO} is the starting frequency, T is the frequency sweep and k_f is the sweep rate.

$$k_f = \frac{BW}{T} \tag{2}$$

where BW is the frequency bandwidth for the sweep and with the two way time (TWT) of the emitted signal calculated as:

$$\Delta t = 2\frac{d}{c} \tag{3}$$

where d is the distance between the antenna and the reflecting target and c is the speed of light in the medium of propagation. Therefore, due to the observed delay in return signal, the return frequency compared to the emitted frequency will be:

$$f_{\mathrm{RF\ received}} = f_{\mathrm{RFO}} + k_f * (t - \Delta t)\,,\ \Delta t \leq t \leq T + \Delta t \tag{4}$$

The difference in frequency (Δf) between the emitted and received signal is therefore:

$$\Delta f = k_f * (-\Delta t) \tag{5}$$

It is this difference in frequency that is output from the detector as data. The negative time of flight can be taken as a magnitude, allowing for the expression:

$$\Delta f = \frac{BW}{T} * 2\frac{d}{c} \tag{6}$$

Due to the relationship expressed in (6), the z-axis distance between the sensor and sandstone sample is kept constant at 100 mm. Thereby, any signal variation can be attributed to rock properties and an ideal reflector can be used to provide a theoretical maximum return signal. The properties of the material that influence the signal parameters are outlined in section II/B.

B. DIELECTRIC THEORY AND APPLICATION OF FREQUENCY MODULATED CONTINUOUS WAVE RADAR TO DIELECTRIC MEDIA

In this section we examine the primary return signal parameters. K-band analysis over a continuous sweep in frequency offers key advantages over a pulsed, single frequency method. These advantages are: improved signal to noise characteristics due to a broader frequency range, a lower intermediate frequency (IF) and relative immunity to harsh ambient conditions.

Dielectric relaxation processes govern wave attenuation and dispersion within dielectric materials, as defined by the complex relative permittivity, ε_r^*. These relaxation processes are influenced by the frequency of the incident radiation, where constituent materials throughout the component scale range dampen localised oscillations. The multiple relaxation modes acting simultaneously within an irradiated material generate significant non-linearity and can complicate data analysis. However, the information provided by this complex return signal allow for feature extractions indicative of the dielectric material properties, inferring a relationship to structural and compositional features of the material; thus FMCW analysis should also be sensitive to the grain/pore size and composition. In sandstones, the relative permittivity is affected by many factors, including; pore fluid types and phase, value of porosity, abundance of high-permittivity mineral inclusions and grain-long axis orientation, all defined by dielectric relaxation [13]. Previous experimentation conducted by the authors focused on the use of X and K-band FMCW to generate a signal response specific to the presence of water or oil within a geomaterial [14]–[16]. It is well documented that K-band radiation undergoes significant attenuation due to heavy absorption at these frequencies, specifically centred around 22.5 GHz, due to the radiation absorption by water. This effect has led to the partitioning of the K-band into the Ku and Ka bands (12-18 GHz and 26.5–40 GHz respectively).

Equation (7) represents the complex component form of ε_r^*, the relative electrical permittivity of a particular medium. ε', represents the observed and real relative permittivity of the material. The imaginary component, $j\varepsilon''$, denotes the ''loss factor'' of the material and therefore represents the dispersion of incident radiation due to conduction and relaxation of atomic constituents.

$$\varepsilon_r^* = \varepsilon' + j\varepsilon'' \tag{7}$$

In many theoretical instances, the imaginary component of this relationship is ignored, as materials used for dielectric media tend to be poor conductors. However, applications within geomaterial samples could be contrary to this assumption, as most radar applications are unable to be reduced into a generic form, especially in the presence of multimodal radar instruments [17], and with many constituent parts of a rock matrix and void spaces offering appreciable conduction, for example, the presence of brines, water and mineral inclusions [18]. Nevertheless, for simplicity, this model operates under the assumption that the component of dielectric loss; the imaginary term, $j\varepsilon''$,in (7) is much smaller than the real component, representing the reflection data.

In principle, detailed knowledge of rock characteristics would lead to the ability to model the response, which could be compared against future measurements. Within section III we introduce previous work, forming a brief literature survey of microwave FMCW use in fields analogous to the intended application of this work and the properties of geomaterials.

III. PREVIOUS WORK

Microwaves within the K-band represent a non-destructive and non-contact means of analysis, with the potential to reveal intrinsic properties of the rock target. FMCW technology has seen wide application within the industrial and automotive sectors for distance and velocity sensing [19], [20]. Millimetre FMCW radar has been successfully applied in defence roles, such as concealed weapon and explosive detection, surveillance and perimeter security and roadside device detection [11]. FMCW radar has also seen use in medical imaging and research, with a proven capability to detect displacement at the μm level for respiration and heartbeat monitoring [21]–[23]. However, the key research elements undertaken to date that are of most relevance to this study are as follows:

A. CORROSION UNDER INSULATION

Corrosion under insulation is an inherent issue with the use of steel core pipelines in downstream oil and gas production, leading to the eventual failure of high value infrastructure assets, if left unchecked. Work to date focuses on the use of the pipeline cladding assembly acting as a coaxial waveguide to influence and direct the propagation of microwave radiation. The pipeline acts as an inner conductor and the cladding acts as an outer conductor, with the thermal insulation between these two conductors acting as a dielectric medium. Working on the principle that water ingress into the pipeline cladding induces a large change in dielectric impedance, a propagating wave will be affected/reflected by this region of high relative permittivity, due to the high real component of the relative permittivity of water in the K-band microwave range. This ''blockage'' of the waveguide acts as an indicator that water ingress has occurred, posing a threat to the integrity of the pipeline asset via oxidation, and analysis of the reflected wave further indicates the distance travelled by the propagating wave, via the application of a fast Fourier transform to the time domain signal data, allowing for the rapid and accurate location of the cladding failure [24]–[26].

B. FREQUENCY MODULATED CONTINUOUS WAVE RADAR FOR SNOW THICKNESS STUDIES

Investigations into the application of K-band FMCW as a tool for research into snow and ice properties have provided data relating to layering, density, water equivalence, total snow height and moisture content [27]–[36]. A summary of key publications in FMCW snow research is given

in Table 1. However there has been little or no research into the application of this technology to rocks and the authors believe that the results reported in this paper represent the potential for a new instrument for dynamic and quasi-static rock analysis and a first for FMCW radar electronics in this role. These multi-disciplinary applications indicate that there is potential for FMCW radar to return significant information about the constituent materials and their arrangement within a rock sample. This applies to distinct grains, to cement and to the fluids (gas and liquid) within the pore space network, via analysis of the dielectric response to incident microwave radiation, delivering a step-change in rock characterisation.

TABLE 1. Summary of previous snow research by radar parameters and measurands.

Lead Author	Galin [31, 32]	Yan [33]	Ayhan [34]	Kwok [35]	Panzer [36]
Year	2008, 2012	2017	2017	2011	2013
Frequency (GHz)	2 to 8	2 to 18	80	2 to 8	2 to 8
Band(s)	S, C	S, C, X and Ku	W	S, C	
Deployment	Airborne		Ground		Airborne
Measurand	Thickness	Snow stratigraphy	Thickness		
Resolution	37.5 mm	14 mm	15 mm	50 mm	50 mm

C. ANALYSIS OF GEOMATERIALS USING FREQUENCY MODULATED CONTINUOUS WAVE RADAR

An assessment of FMCW signal return in the K-band was conducted on eight rock samples in [14] and [16] with the results indicating clear differences in relative permittivities between these materials. Previous work by the first author has resulted in the following, key observations:

- Qualitatively, we can distinguish between different sandstone samples in an ambient laboratory environment (herein referred to as ''room-dry''), where the observed signal reflection amplitudes extracted via Fourier transforms, where water content represents both laboratory air moisture content and partially water-saturated sandstones
- It is possible to discern room-dry and partially kerosene-saturated sandstone samples
- It is possible to distinguish between partially water-saturated and partially kerosene-saturated sandstone samples
- Mineralogy plays a major role in return signal quality
- Degree of grain shape and orientation anisotropy and heterogeneity play a major role in return signal quality

Informed by this work, the research direction was adapted to evaluate two sandstones of approximately homogeneous bulk mineralogy and two sandstones with observed material heterogeneity and anisotropy.

IV. DIELECTRIC THEORY APPLIED TO GEOMATERIALS AND RESULTING MODELS

Using well-documented previous work in snow and corrosion under insulation studies as analogues and potential validation of the FMCW technique to identify features, results have been obtained through laboratory-based experimental work in the novel application of the FMCW technique to geomaterial analysis. This work has focused on the differentiation of pore content in quartz-rich porous sandstone samples, with properties analogous to reservoir-grade rocks. The following sections will outline the theory, experimental technique, equipment and calculated values of relative permittivity from reflected microwave radiation in both the X and K-bands.

A. SERIES AND PARALLEL LAYER MODELS

The application of dielectric theory to geomaterial properties is not a new innovation, with layer models and mixing rules dating to the 1930's. This section provides an overview of layer models and inclusion models for later application in this work.

Voigt and Reuss' concept [37] describes the simplest generalised forms (upper and lower limitations of ε_r^*) of a geomaterial consisting of n components, where each layer represents a specific rock constituent. A volume factor, V_i, gives the relative thickness of each layer.

1) PARALLEL MODEL

For parallel models, where the electric field is parallel to the boundary plane between geomaterial components:

$$\varepsilon_{r,\parallel}^* = \sum_{i=1}^{n} V_i \cdot \varepsilon_{r,i} \tag{8}$$

$$\varepsilon_{r,\parallel}^* = (1-\phi)\,\varepsilon_{r,ma} + \phi \cdot \varepsilon_{r,fl} \tag{9}$$

2) SERIES MODEL

For series models, where the electric field is perpendicular to the boundary plane between geomaterial components:

$$\varepsilon_{r,\perp}^* = \left[\sum_{i=1}^{n} Vi \cdot \varepsilon_{r,i}^{-1}\right]^{-1} \tag{10}$$

$$\varepsilon_{r,\perp}^* = \left[(1-\phi)\,\varepsilon_{r,ma}^{-1} + \phi \cdot \varepsilon_{r,fl}^{-1}\right]^{-1} \tag{11}$$

In each case, ϕ is the measured sample porosity, V_i is the volume fraction and $\varepsilon_{r,i}$ is the i^{th} value of the relative permittivity. $\varepsilon_{r,ma}$ is the relative permittivity of the geomaterial matrix and $\varepsilon_{r,fl}$ is the relative permittivity of a single phase pore fluid. These equations represent the form of the upper and lower permissible limits for the dielectric strength of a porous rock, respectively $\varepsilon_{r,\parallel}^*$ and $\varepsilon_{r,\perp}^*$.

The amalgamation of series and parallel models provides an arithmetic mean: the Voigt-Reuss-Hill average, equation (12).

$$\varepsilon_{r,H}^* = \frac{\varepsilon_{r,\parallel}^* + \varepsilon_{r,\perp}^*}{2} \tag{12}$$

The Lichtnecker and Rother generalisation [18]

$$\varepsilon_r^* = \left[\sum_i V_i \left(\varepsilon_{r,i}^{\alpha}\right)\right]^{\frac{1}{\alpha}} \tag{13}$$

The Lichtnecker and Rother generalisation (1931), equation (13) is an expression of combined individual equations, where α can be considered a "texture parameter" and $-1 < \alpha < 1$. A α-value of -1 represents the series model and a α-value of 1 represents the parallel model. For a fully saturated porous structure, this becomes:

$$\varepsilon_r^* = \left[(1-\phi)\left(\varepsilon_{r,ma}^{\alpha}\right) + \phi \cdot \left(\varepsilon_{r,fl}^{\alpha}\right)\right]^{\frac{1}{\alpha}} \tag{14}$$

3) COMPLEX REFRACTIVE INDEX METHOD

Wyllie's time average equation allows for the derivation of the complex refractive index method (CRIM) formula [18], [38]. Wyllie's equation can be described as the sum of EM signal travel times during propagation through both the host medium and the inclusions/fluids contained therein. The general expression in terms of inverse velocity (or slowness) is,

$$\frac{1}{v} = \frac{1}{v_{vacuum}} \cdot \sqrt{\varepsilon_r^*} \tag{15}$$

where,

$$\frac{1}{v_{vacuum}} = \frac{1}{c} = 3.36\ \text{nsm}^{-1}) \tag{16}$$

thus,

$$\frac{1}{v_{CRIM}} = (1-\phi)\frac{1}{v_{ma}} + \phi \cdot \frac{1}{v_{fl}} \tag{17}$$

where $\frac{1}{v_{ma}}$ is the matrix slowness and $\frac{1}{v_{fl}}$ is the fluid slowness, leading to the calculation of the relative permittivity of a composite material,

$$\varepsilon_{r,CRIM}^* = \left((1-\phi)\sqrt{\varepsilon}_{r,ma} + \phi \cdot \sqrt{\varepsilon}_{r,fl}\right)^2 \tag{18}$$

or, more generally,

$$\varepsilon_{r,CRIM}^* = \left[\sum_{i=1}^{n} V_i \cdot \varepsilon_{r,i}^{-\frac{1}{2}}\right]^2 \tag{19}$$

It can be seen that the generalised CRIM equation (19) is identical to the Lichtnecker and Rother equation (13) with a α value of 0.5.

Thus, for a simplified, partially fluid-saturated and uniform, porous sandstone,

$$\varepsilon_{r,sa}^* = \left[\left(1-\phi_T\sqrt{\varepsilon}_{r,ma}^*\right) + \left(\phi_f\sqrt{\varepsilon_{r,fl}^*} + \phi_a\sqrt{\varepsilon_{r,air}^*}\right)\right]^2 \tag{20}$$

where $\varepsilon_{r,sa}^*$ is the observed relative permittivity of the investigated sample, ϕ_T is the total measured sample porosity, ϕ_f is the fractional porosity occupied by fluid (determined by measured differences in sample mass following fluid immersion), ϕ_a is the fractional porosity occupied by air, $\varepsilon_{r,fl}$ is the relative permittivity of a single phase pore fluid, $\varepsilon_{r,air}$ is the relative permittivity of the volumetric air content and $\varepsilon_{r,ma}$ is the relative permittivity of the geomaterial matrix [39]. This is an idealised situation and is unrepresentative of the impurities to be found in typical sandstones. Therefore (20) should also account for observed mineral types within the samples under investigation. In the case of all sandstone samples tested in this study, this would include mica, clays and feldspars but many other minerals are also likely to be present in typical sandstones, such as pyroxenes, different forms of iron oxides and hydroxides and sulphides [40]. In principle, detailed knowledge of the geomaterial characteristics would lead to the ability to model the response, which could be compared against measurements.

While models that account for sphericity and angularity of grains contained within a sandstone sample and their effect on reflected radiation exist, this paper will not describe these models in depth. However, the apparent bulk measurement of a sample will contain an indication of the mean sphericity of that sample, with a planar-sided clast represented by the Series Model (10) and (11) and an entirely spherical arrangement of clasts represented by the Voigt-Reuss-Hill mean (12), as discussed in section IV/A/2. Both of these arrangements are unrealistic in nature but represent two idealised modelling extremes that offer insight into the variations in return signal imposed by the shape of both rock matrix and mineral inclusions [18]. Qualitatively, the mean sphericity of a sample can be inferred from the magnitude of the reflection coefficient, Γ, if all other factors are known.

V. EQUIPMENT AND SAMPLE CHARACTERISATION

In order to ensure data confidence and consistency, the antenna radiation pattern and geomaterial sample mineralogy require calibration and quantification. The apparatus used to analyse the antenna characteristics was an azimuth/elevation dual translation stage coupled to NSI 2000 antenna measurement software (version 4.12.45).

A. ANTENNA CHARACTERISATION

In order to inform an appropriate geomaterial response for this antenna setup, the radiation output was determined as a function of bandwidth sweep. To meet this requirement, three scans were performed using a two-dimensional translation stage coupled to an OEWG (open-ended waveguide) standard probe, type WR42, for the K-band (18-26.5 GHz) and using a non-radiative near-field separation distance between the probe and the antenna under test (AUT) of 100 mm. Data sets were acquired representing the 1500 MHz bandwidth sweep for the frequency band. Figure 1 shows the radiation pattern acquired for a Flann K-band antenna (model: #21240-20/ serial: #219405) and acts as a control measurement for both amplitude and phase.

B. GEOMATERIAL CHARACTERISATION

Acquired from Stancliffe Stones of Alfreton, UK, four sandstone samples (100 mm x 100 mm x 12 mm) were tested, with sample size informed by parameters determined by antenna characterisation techniques, specifically the peak spot size on the sample. The samples are: Darney, Lazonby, Locharbriggs and Red St. Bees sandstones. These samples were chosen for their well-documented properties and to represent a varying range of mineralogical and textural complexities (e.g. homogenous vs. layered). Each sandstone sample possesses approximately uniformly distributed bulk mineralogy

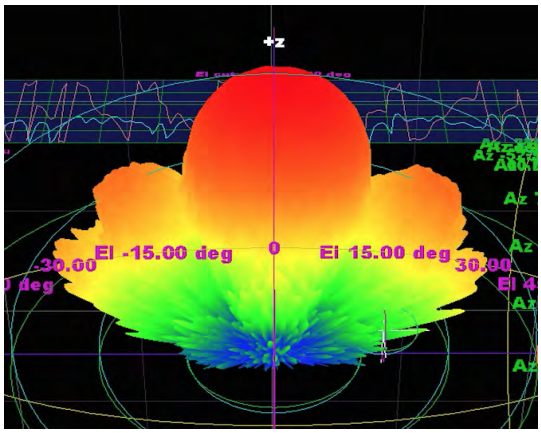

FIGURE 1. Radiation pattern for K-Band Flann Microwave antenna model 21240-20.

and also contains discernable differences in grain orientation, distribution and in the sample porosity and pore space characteristics, offering a unique and repeatable return intermediate frequency (IF) waveform. Petrographic descriptions of these samples are given in Section V/B/1.

1) ENERGY DISPERSIVE X-RAY ANALYSIS AND GSE/BSE IMAGING

An important factor in the return signal used to derive relative permittivity values is the presence of metallic (or highly conductive) mineral compounds within the sandstone sample. In order to define individual rock characteristics that may subsequently affect relative permittivity measurements, energy-dispersive X-ray (EDX) combined with backscatter electron (BSE) and gaseous secondary electron imaging were performed on each sandstone sample. These analytical techniques provide both a chemical fingerprint and a high definition image of rock grain/matrix constituents within a two-millimetre field of view, as performed on polished thin sections for each sample. These techniques allow for the quantification of the elements present within the samples and are presented as a function of elemental atomic weight percentages (table 2) Data was acquired using a Quanta650 field emission gun (FEG) scanning electron microscope (SEM) with Oxford Instruments EDX detector. EDX data were further developed using the Oxford Instruments AZtec Software package (version 3.3). Sample characterisation images for Darney, Lazonby, Locharbriggs and Red St. Bees sandstones are presented in figures 2-4. EDX mapped potassium, sodium, calcium and aluminium, in addition to the relative intensities within the sample, occupy the volumes containing feldspar and clays; orthoclase feldspar ($KSiAl_3O_8$) and plagioclase feldspar end members albite ($NaSiAl_3O_8$) and anorthite ($CaSi_2Al_2O_8$) and aluminium silicate clays $(Al,Si)_3O_4$ [40].

a: DARNEY SANDSTONE

Analysis of the Darney sandstone shows that it consists predominantly of moderately well-sorted, spheroidal, sub-rounded to rounded quartz (SiO_2) grains with a fine to medium grain size (125 – 350 μm) [41], with subsidiary orthoclase feldspar and clay (kaolinite) and a porosity of 18.7% [42]. Figure 2A is a composite false colour image overlaying the relative magnitudes of characteristic x-rays for each element recorded. Each detected element is represented by assigned colours, with dark regions representing pore spaces. The orthoclase feldspar can be identifed as distinct, angular and often fractured grains, rich in aluminium and potassium. This sample is relatively free of high permittivity metallic inclusions that would affect the apparent dielectric strength, however figure 2A illustrates the presence of iron within some kaolinite-filled pores. Figure 3A, a BSE image measuring material greyscale contrast due to atomic number, shows variablility in grainsize (note magnification is uniform throughout figures 2 and 3), porosity, feldspar content and iron-rich particles. Figure 4A shows the high definition GSE image of the sample and highlights grain-supported rock fabric with some quartz overgrowth observed.

TABLE 2. Elemental constituent percentages acquired by EDX analysis and expressed in atomic weights for each sandstone thin section.

%	Darney	Lazonby	Locharbriggs	Red St. Bees
Carbon	43.9	43.2	46.7	42.6
Oxygen	42.4	41.9	40.4	42.5
Silicon	12.9	13.8	11.6	12.2
Aluminium	0.7	0.6	0.8	1.3
Potassium	0.1	0.4	0.3	0.5
Iron	<0.1	<0.1	0.1	0.2
Magnesium	<0.1	<0.1	0.1	0.2
Calcium	<0.1	<0.1	<0.1	0.1
Sodium	<0.1	<0.1	<0.1	0.2
Titanium	<0.1	<0.1	<0.1	~0.1

b: LAZONBY SANDSTONE

Characterisation of the Lazonby sandstone (composite image in figure 2B) shows that this sample contains predominantly quartz and orthoclase feldspar with some clays, in much the same proportions as the Darney sandstone. However the iron content, while similar in magnitude to the Darney sandstone (table 2), is more dispersed throughout the sample. Dominated by grain-supported, fine to medium-sized spheroidal, sub-rounded/rounded grains and well-sorted quartz clasts, ranging between 200-500 μm (figure 3B), the observed porosity at 11.6% is significantly lower than the other samples analysed for this study [43]. This porosity reduction can be attributed to significant syntaxial quartz overgrowth, clearly visible in figure 4B.

c: LOCHARBRIGGS SANDSTONE

Consisting of well-sorted, very fine to fine (100 – 250 μm), sub-rounded to rounded grains (figure 2C) and a porosity of 26% [44], the Locharbriggs sandstone contains grains of angular orthoclase feldspar, as determined by the

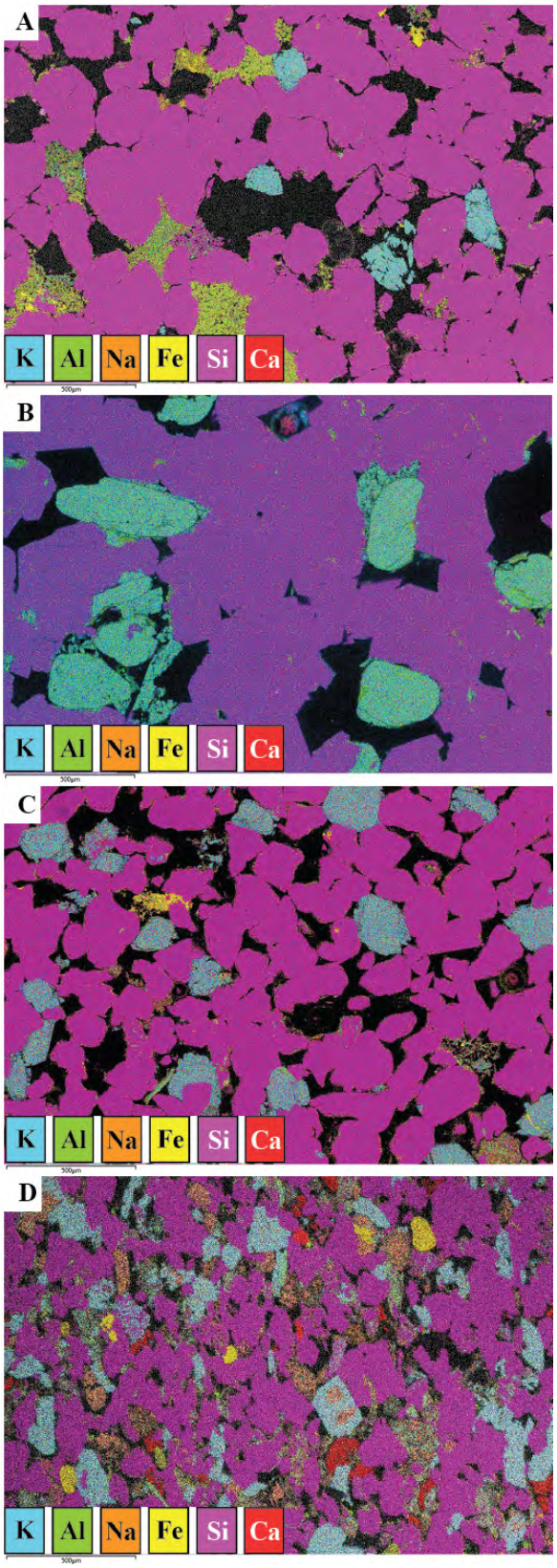

FIGURE 2. Energy dispersive x-ray (EDX) analysis images showing colour-coded presence of potassium, aluminium, sodium, iron, silicon and calcium, where present.

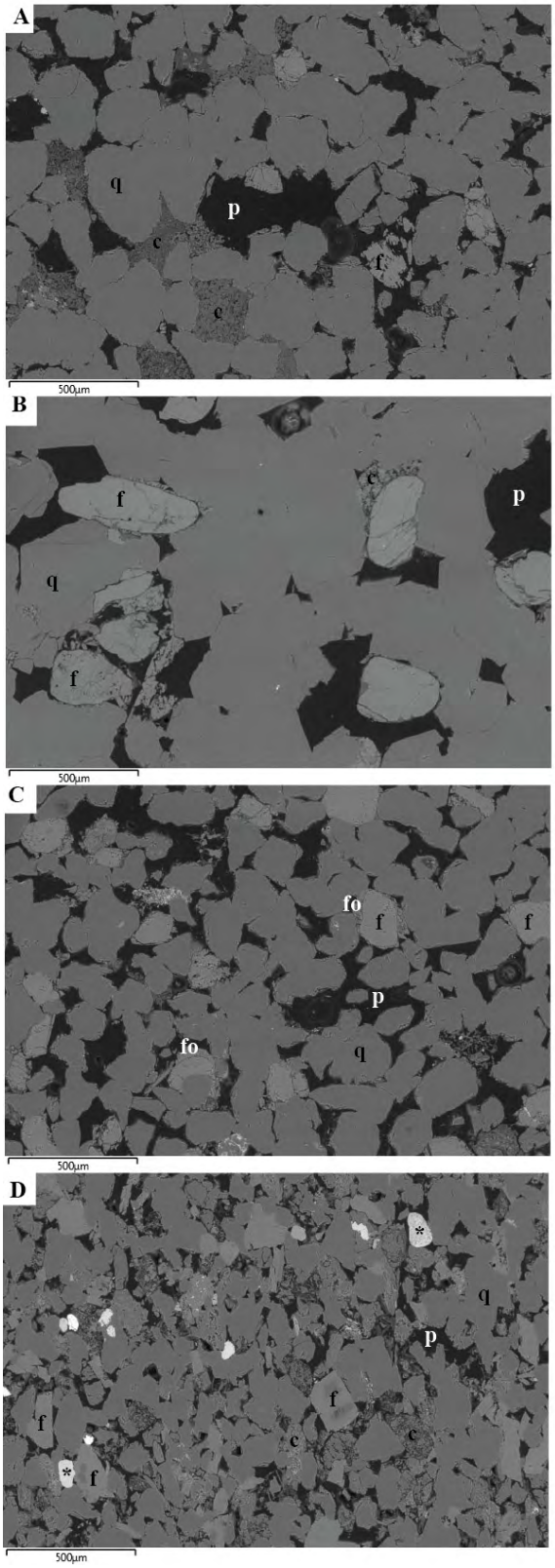

FIGURE 3. Backscattered electron (BSE) images. A= Darney sandstone, B= Lazonby sandstone, C= Locharbriggs sandstone and D= Red St. Bees sandstone. Key: p = pore, q = quartz, f = feldspar, fo = feldspar overgrowth, c = clay, ∗ = iron-rich particles.

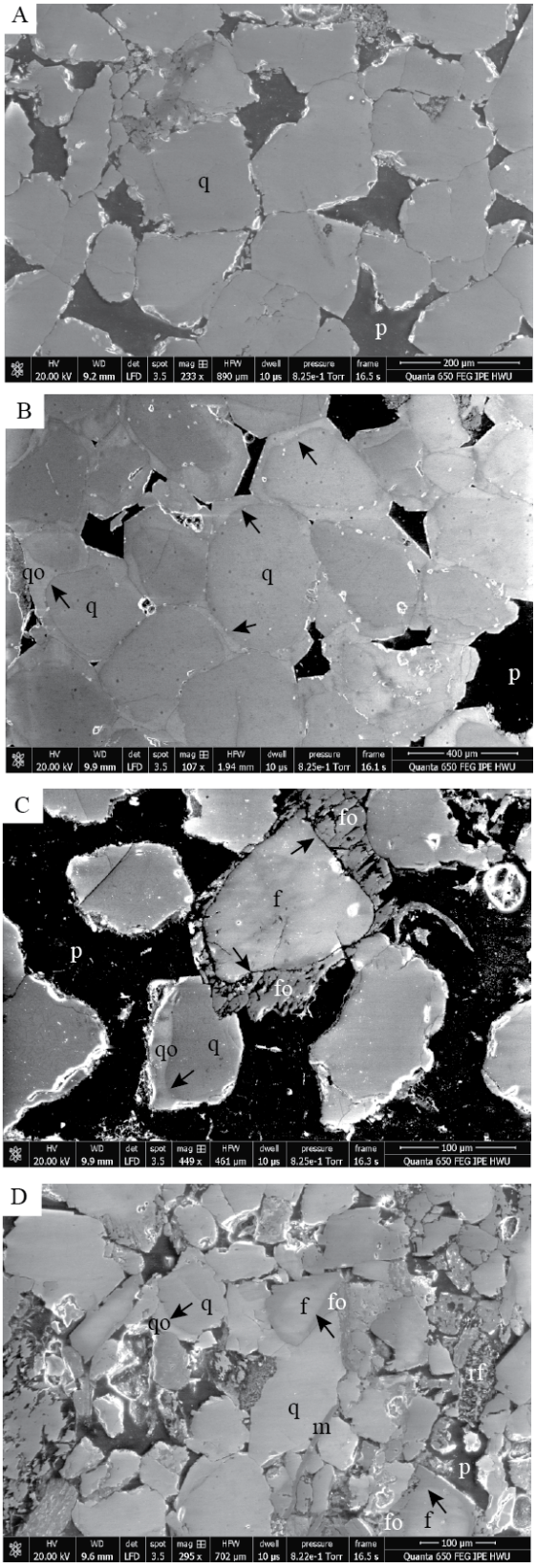

FIGURE 4. Gaseous secondary electron (GSE) images. A= Darney sandstone, B= Lazonby sandstone, C= Locharbriggs sandstone and D= Red St. Bees sandstone. Key: p = pore, q = quartz, qo = quartz overgrowth, f = feldspar, rf = rotten feldspar, fo = feldspar overgrowth, c = clay, m = mica.

co-occurance of aluminium and potassium, corroborated by the BSE analysis shown in figure 3C. Figure 2C also shows a marginal iron content within some pore-filling clays. The GSE image shown in figure 4C illustrates the grain-supported nature of the rock fabric, the crystalline structure of the feldspar overgrowths due to visible cleavage, with little evidence of quartz overgrowth or porosity reduction.

d: RED ST. BEES SANDSTONE

The Red St. Bees sandstone sample (figure 2D) displays a larger variety of constituent minerals when compared to the other samples within this study. With sub-angular to sub-rounded, very-fine to fine sized grains (50 – 200 μm) and a porosity of 21.3% [45], this sample has a notably diverse mineralogy and contains the highest levels of metallic elements of all the samples characterised, specifically for potassium, calcium, sodium and aluminium (confirming the presence of both orthoclase and plagioclase feldpsars in addition to abundant clays). Also visible within figure 2D is the presence of mica, calcium phosphate and dolomite. Iron, magnesium and titanium are also present in measurable quantities (table 2). Figure 3D, a high definition BSE image, illustrates the highly angular quartz clasts, feldspar grains with feldspar overgrowths and pore-filling clays. Some feldspar overgrowths are also clearly visible in figure 4D in addition to the formation of secondary porosity due to identification of feldspar weathering or ''rotten feldspar''.

C. EXPERIMENTAL SETUP AND PROCEDURE

Illustrated in figure 5, the experimental setup and procedure can be divided into 6 main stages:

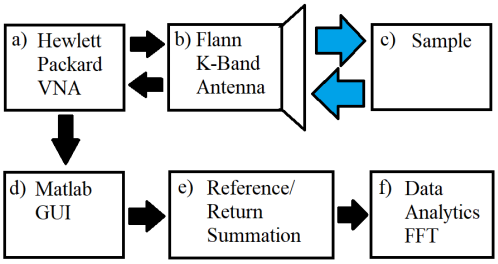

FIGURE 5. Block diagram of experimental setup.

a) The apparatus used to create the FMCW signal was a Hewlett-Packard/Keysight 8510 Vector Network Analyser. Each FMCW waveform generated had a bandwidth of 1500 MHz, from 24 – 25.5 GHz, with a chirp duration of 300 milliseconds.

b) Flann Microwave model 21240-20 standard gain horn antenna with manufacturer serial number 219405, capable of radiation output ranging 17.6 - 26.7 GHz and with a nominal gain of 20 dBi (at 22.15 GHz), as characterised in section V/A. This antenna was affixed to a static mounting and directed onto the sandstone samples maintaining a separation distance of 100 millimetres.

c) Sandstone samples of Darney, Lazonby, Locharbriggs and Red St. Bees both room-dry and partially saturated

TABLE 3. Partial water saturation values expressed as a percentage of occupied pore space for Darney, Lazonby, Locharbriggs and Red St. Bees sandstones following room dry and partially-saturated mass measurements. Soak time of 96 hours.

Sample	Porosity volume occupied by deionised water (%)
Darney	56.76
Lazonby	58.67
Locharbriggs	59.64
Red St. Bees	56.23

(Table 3) were selected. The four sandstone samples were weighed prior to immersion in deionised water for 96 hours. Following extraction from the deionised water, each sample was briefly placed on absorbent paper to remove excess fluid from the sample surface/interface. The samples were again weighed to determine the mass of fluid uptake, from which the magnitude of the water saturation was determined prior to alignment in front of the sensor. Note this technique will not achieve 100% water saturation

d) Graphical User Interface via Matlab 2017a.

e) Summation of reference signal to return signal waveforms to generate intermediate frequency (IF).

f) Application of data analytical processes to interrogate sample acquisition data into frequency domain. This is achieved by application of a Fourier transform, from which amplitude and phase extractions are performed. Data was taken from the same scanning position, corresponding to the amplitude peak of the central lobe of radiation output from the relevant band antenna, in this case 100 mm from the antenna aperture. Calculation of the reflection coefficient was taken via the ratio of the radiation intensity peak, $I_{incident}$, measured for the control sample (copper sheet acting in the role of an ideal reflector) and the radiation return signal, $I_{reflected}$, acquired by the K-band antenna [46]. Thus,

$$\Gamma = \frac{I_{reflected}}{I_{incident}} = \frac{(n_1 - n_2)^2}{(n_1 + n_2)^2} \tag{21}$$

Solving equation (21) for n_2 gives the average refractive index of the sandstone sample as the propagating wave transits from the free-space medium with refractive index n_1.

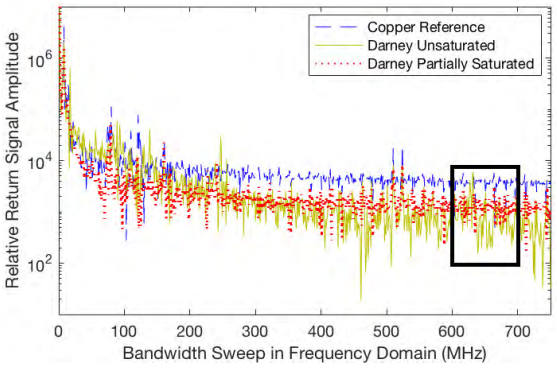

FIGURE 6. Return signal amplitudes, extracted via Fourier transform, for room-dry and partially water saturated Darney sandstone with copper sheet acting as an ideal reflector.

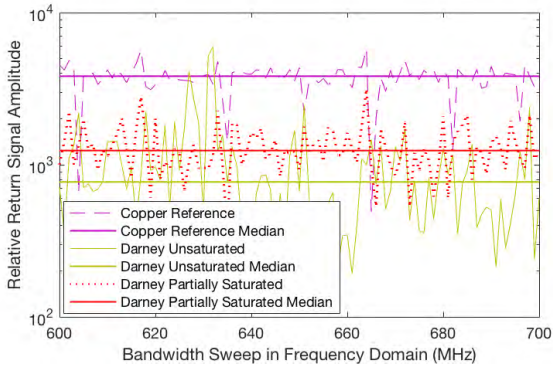

FIGURE 7. Return signal amplitudes for room-dry and partially water saturated Darney sandstone, with copper sheet acting as an ideal reflector, and with data medians indicated over a 100 MHz sample size (between 600-700 MHz bandwidth sweep, see Figure 6).

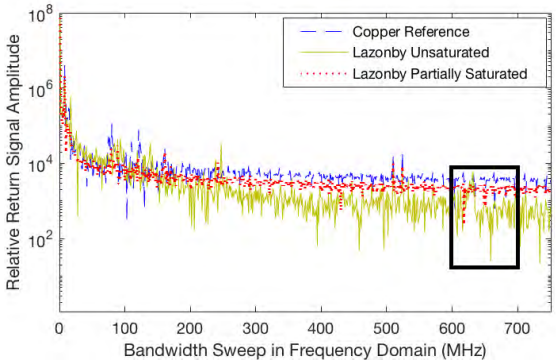

FIGURE 8. Return signal amplitudes, extracted via Fourier transform, for room-dry and partially water saturated Lazonby sandstone with copper sheet acting as an ideal reflector.

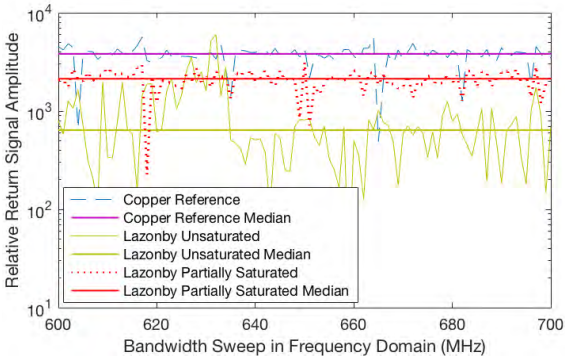

FIGURE 9. Return signal amplitudes for room-dry and partially water saturated Lazonby sandstone, with copper sheet acting as an ideal reflector, and with data medians indicated over a 100 MHz sample size (between 600-700 MHz bandwidth sweep, see Figure 8).

VI. RESULTS

Return signal waveforms are given in Figures 6 and 7 for Darney Sandstone, figures 8 and 9 for the Lazonby Sandstone, figures 10 and 11 for the Locharbriggs sandstone and figures 12 and 13 giving the return waveforms for the Red St. Bees sandstone. All figures listed above are presented in the frequency domain. The acquired values for K-band refractive index and overall relative permittivities for room-dry and partially saturated samples are shown in Tables 4 and 5

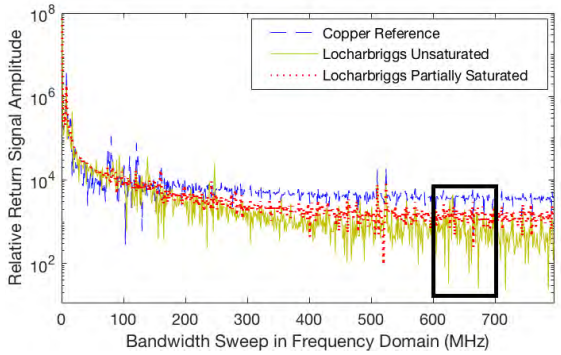

FIGURE 10. Return signal amplitudes, extracted via Fourier transform, for room-dry and partially water saturated Locharbriggs sandstone with copper sheet acting as an ideal reflector.

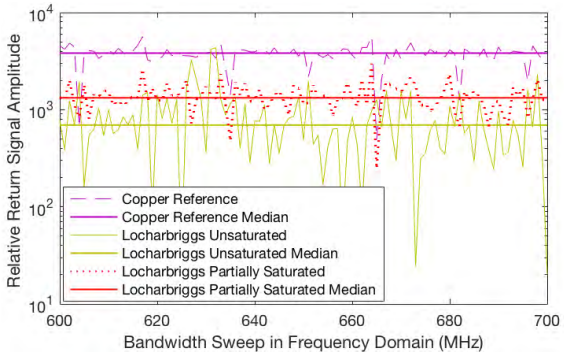

FIGURE 11. Return signal amplitudes for room-dry and partially water saturated Locharbriggs sandstone, with copper sheet acting as an ideal reflector, and with data medians indicated over a 100 MHz sample size (between 600-700 MHz bandwidth sweep, see Figure 10) .

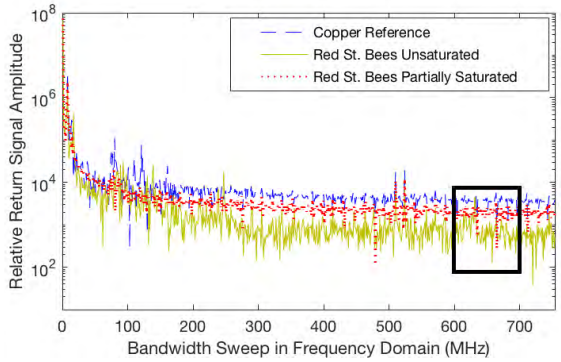

FIGURE 12. Return signal amplitudes, extracted via Fourier transform, for room-dry and partially water saturated Red St. Bees sandstone with copper sheet acting as an ideal reflector.

respectively and are expressed as the derived rock relative permittivity from the CRIM equation (20) rearranged for $\varepsilon^*_{r,ma}$ to give,

$$\varepsilon^*_{r,ma} = \left[\frac{1-\left[\sqrt{\varepsilon^*_{r,sa}}-\left(\phi_f\sqrt{\varepsilon^*_{r,fl}}+\phi_a\sqrt{\varepsilon^*_{r,air}}\right)\right]}{\phi_T}\right]^2 \quad (22)$$

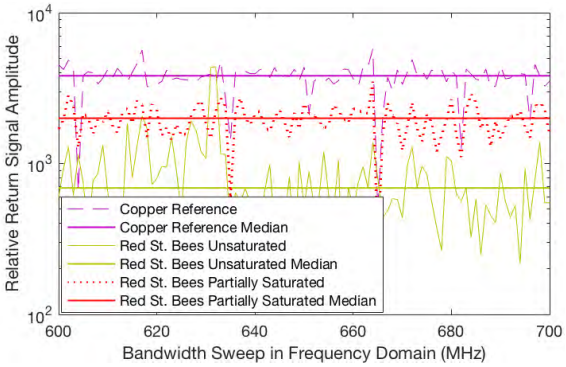

FIGURE 13. Return signal amplitudes for room-dry and partially water saturated Red St. Bees sandstone, with copper sheet acting as an ideal reflector, and with data medians indicated over a 100 MHz sample size (between 600-700 MHz bandwidth sweep, see Figure 12).

TABLE 4. Data acquired from K-band measurement of room-dry sandstone samples and calculated values for reflection coefficient, refractive index, relative permittivity and complex refractive index method.

Symbol	Darney	Lazonby	Locharbriggs	Red St. Bees
Γ	0.20	0.17	0.18	0.18
η_2	2.6	2.4	2.5	2.5
ε^*_r	6.76	5.76	6.25	6.25
ϕ	0.187	0.12	0.26	0.213
CRIM (22)	2.97	2.59	3.03	2.91

TABLE 5. Data acquired from K-band measurement of partially saturated sandstone samples and calculated values for reflection coefficient, refractive index, relative permittivity and complex refractive index method.

Symbol	Darney	Lazonby	Locharbriggs	Red St. Bees
Γ	0.32	0.56	0.35	0.52
η_2	3.6	6.95	3.9	6.20
ε^*_r	12.96	48.30	15.21	38.44
ϕ	0.187	0.12	0.26	0.213
CRIM (22)	5.63	8.56	7.00	9.37

A. APPLICATION OF LAYERING MODELS

The mathematical descriptions used so far for this work have focused on homogeneous/isotropic materials. This is unrealistic and not representative of the constituent properties of most rocks, as many rocks are porous, their mineralogy is variable and they tend to be layered. Therefore the overall model highlights the need to perform in-depth microwave propagation modelling through porous/saturated media. Application of the CRIM for the averaged nature of the observed refractive index of both the air-filled pore spaces within the samples and the rock grain-cement system under investigation offers a correlation between return signal from a dry or partially saturated sample with respect to the dielectric strength of the geomaterials present.

VII. DISCUSSION

From previous studies [15], [16], the following effects were expected and were observed:

- Same response for Cu sheet for each FMCW acquisition
- Consistent and repeatable results (each acquisition repeated ten times with each acquisition confirming consistency of results).
- Presence of fluid increases $\varepsilon^*_{r,sa}$ as a function of ϕ_T and saturation percentage due to increased reflection coefficient, Γ
- ϕ_T affects $\varepsilon^*_{r,sa}$ in room-dry samples
- High metallic inclusion content correlates to high $\varepsilon^*_{r,sa}$
- Presence of quartz overgrowth potentially correlates to high $\varepsilon^*_{r,sa}$ due to planar grain boundaries increasing reflection coefficient, Γ

Using values of relative permittivity, ε_r, as stated in literature for the physical properties of geomaterials, with pure quartz stated to have a relative permittivity of 4.5 – 4.7 (see table 6) [18], [47], analysis of the data suggests that, taking into account the impurities contained within the sandstone samples (i.e. not pure quartz with quartz overgrowths but a composite of quartz, mica, feldspar, other conductive minerals and mineral cements, normally quartz and calcite ($CaCO_3$)), the measured relative permittivity values for all samples lie within an appropriate range, with differences attributable to variations in sample mineralogy. Note that the data presented within table 6 was acquired at an investigation frequency of 1 GHz [18], [47]. The use of these relative permittivity values in this work is taken as a general indication of the qualitative differences in expected values.

TABLE 6. Representative Relative Permittivity Values for Common Geomaterials at approximately 1 GHz.

Substance	ε^*_r (@ ~1 GHz)
Quartz	4.5-4.7
Dry Sand	4
Water-saturated Sand	25
Calcite	6.4-8.5
Gas	1
Water	80
Natural Oil	2.0-2.4
Quartz	4.5-4.7

The mineral composition of the sandstone samples, acquired via EDX analysis, show a correlation between the presence of high conductivity mineral inclusions and a high complex relative permittivity measurement within the Lazonby and Red St. Bees sandstones. The low porosity value together with the presence of aluminium and potassium within the feldspar and clay content of the Lazonby sandstone infers a higher concentration of conductive inclusions per unit volume. The relative abundance of high permittivity metallic contents of the Red St. Bees sandstone, iron and magnesium in addition to the aluminium and potassium within the feldspars and clays, result in a high measured complex relative permittivity that exceeds the limits imposed by the CRIM model. The ''cleaner'' composition of the Darney and Locharbriggs sandstones is verified by the correlation of these samples to the layering and averaging models discussed in section IV, which do not account for the presence of highly conductive mineral inclusions or clastic angularity.

Using the layering models to extrapolate the relative permittivity of the geomaterial without porosity gives a value of $\varepsilon^*_{r,ma}$ of approximately 9, shown in figure 14. The partially water saturated measurement for relative permittivity of the Lazonby and Red St. Bees sandstones, figure 15, lie above the upper limit as postulated by the layering models. This could be attributed to the presence of a conductive fluid within the samples when saturated and the consequent presence of a greater variety of conductive pathways, when compared to the insulating effect of air-filled pore spaces. It is also notable that the distribution of constituent materials within each sample plays a larger role in the more heterogeneous/anisotropic samples than in the more uniform and isotropic samples composed almost purely of quartz. However, the calculated CRIM values for all sample sandstones are in acceptable agreement for each saturation phase of the experiment and offer potential validation of this free-space and non-invasive sensing method.

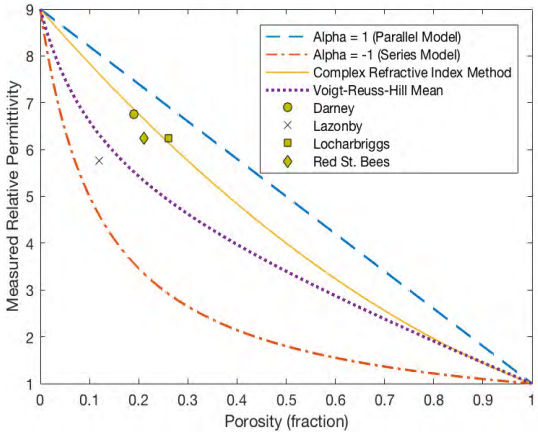

FIGURE 14. Measured room-dry data vs. layering models. $\varepsilon_{r,ma} = 9$ and $\varepsilon_{r,fl} = 1$.

This research has reported on preliminary findings using a unique, free-space method of relative permittivity measurement in the K-Band. The application of layering models and correlation between these models and observed values for ε^*_r can be utilised to infer the following:

This method allows for the identification of magnitude of water saturation present in a sample, as a static measurement, via an expansion of the CRIM equation (20), if bulk porosity and mineral composition (i.e. quartz grains and cement) are known factors.

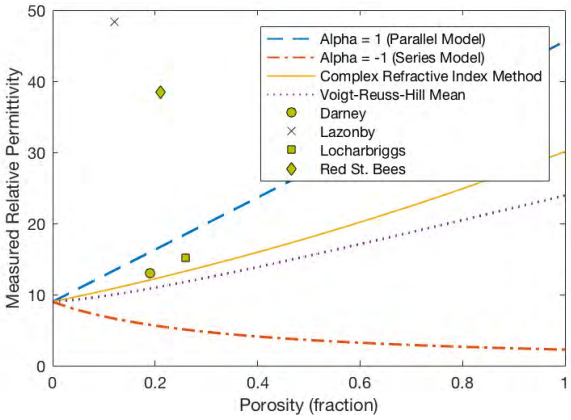

FIGURE 15. **Measured deionised water saturation data vs. layering models. $\varepsilon_{r,ma} = 9$ and $\varepsilon_{r,fl} = 80$.**

It is extremely difficult to get any porous sample 100% water saturated even if it is water wet. If a sample could be 100% water saturated, this method can infer the sample mineralogy in terms of percentage of quartz, mica and feldspar, provided relative permittivity values for the feldspar groups and clays can be accurately obtained for the K-Band, representing, again, a static measurement.

For dynamic measurement, for a ''100% quartz'' rock, with a known porosity and good pore connectivity, water introduced to a room-dry sample under pressure, free space measurement of ε_r^* will allow for the tracking of the resulting flood front of the saturating liquid as a function of time. As the water enters the field of view of the antenna, it will be possible to measure a distinct change in the FMCW return signal, typically a phase shift to the right of the ''dry'' signal and an increase in return signal amplitude. However, this measurement will occur as a bulk measurement, representing an average of the relative permittivity within the field of view of the antenna, necessitating a low antenna/sample separation distance (and/or dielectric lensing to prevent divergence of the microwave radiation).

VIII. CONCLUSION

The seminal results within this paper demonstrate the performance of FMCW inspection and analysis as a means of identifying pore space occupancies within partially saturated sandstones as well as identification of geomaterial properties based on porosity and composition. The presence of deionised water within the sandstone samples is clearly discernable within the calculated values for relative permittivity for each sample, the most extreme being the Lazonby sandstone sample with a bench-top dry relative permittivity of 5.76 and a partially water-saturated (58.67% of porosity volume) relative permittivity of 48.3. These values are in approximate agreement with theoretical values for relative permittivity for dry and partially saturated sandstones. The application of the complex refractive index method provides values of calculated sandstone relative permittivities, for dry and partially saturated specimens. Experimental verification of the analysis was supported by measurements using EDX, BSE and GSE methods. Future work will focus on dynamic real-time analysis of geomaterials, wherein we will aim to exploit the benefits of a non-contact and non-destructive means of tracking pore occupancies, porosity changes and high permittivity mineral presence. Successful validation of FMCW analysis under dynamic loading conditions would be a significant advance for the geoscientist and geomechanicist that can augment and validate current tomographic methods that require samples to be analysed in high radiation environments using static and expensive equipment of extremely limited availability. The application of FMCW in this role offers a means to contribute to the refinement of geomechanical modelling techniques currently employed by research groups dedicated to the understanding of fluid/pore network interactions and the effect these parameters have on rock deformation and fluid flow. The sensitivity of this sensing modality, and its non-contact and non-destructive properties, have the potential to provide near to real-time analysis of geomaterials under varying test conditions and to inform the creation of more accurate geomechanical modelling. Even a 1% enhancement of modelling accuracy has significant impact potential for the field of carbon capture and reservoir management. This research brings a distinct contribution to the flourishing research interest in creating more accurate digital-rock representations. Unlike prior works that seek to explore micro-porosities via microfluidics, our measurements are from real 3D samples with highly sensitive analysis revealing key micro characteristics of the geomaterial.

ACKNOWLEDGMENTS

The authors wish to thank the Energy Technology Partnership (ETP) and Maersk/Total for providing project funding, Marshalls Stancliffe Stone for the provision of specimens of Darney, Lazonby, Locharbriggs and Red St. Bees sandstones.

REFERENCES

[1] W. Song, J. Yao, J. Ma, G. D. Couples, Y. Li, and H. Sun, ''Pore-scale numerical investigation into the impacts of the spatial and pore-size distributions of organic matter on shale gas flow and their implications on multiscale characterisation,'' *Fuel*, vol. 216, pp. 707–721, Mar. 2018.

[2] J. R. Underhill, N. Lykakis, and S. Shafique, ''Turning exploration risk into a carbon storage opportunity in the UK Southern North Sea,'' *Petroleum Geosci.*, vol. 15, pp. 291–304, Oct. 2009.

[3] G. Yielding, N. Lykakis, and J. R. Underhill, ''The role of stratigraphic juxtaposition for seal integrity in proven CO_2 fault-bound traps of the Southern North Sea,'' *Petroleum Geosci.*, vol. 17, no. 2, pp. 193–203, 2011.

[4] D. Chapman and W. Trybula, ''Meeting the challenges of oilfield exploration using intelligent micro and nano-scale sensors,'' presented at the 12th IEEE Int. Conf. Nanotechnol. (IEEE-NANO), Birmingham, U.K.: International Convention Centre, Birmingham, Aug. 2012.

[5] P. Krütli, M. Stauffacher, T. Flüeler, and R. W. Scholz, ''Functional-dynamic public participation in technological decision-making: Site selection processes of nuclear waste repositories,'' *J. Risk Res.*, vol. 13, no. 7, pp. 861–875, 2010.

[6] T. C. Bailey, ''Application of X-band radar to sense hydrocarbon seepage,'' *Oil Gas J.*, vol. 94, pp. 72–75, Dec. 1996.

[7] F. Rocca, ''Remote sensing from space for oil exploration,'' in *Proc. IEEE Int. Geosci. Remote Sens. Symp. (IGARSS)*, Jul. 2015, pp. 2876–2879.

[8] G. A. Morozov, O. G. Morozov, and M. R. Galimov, "Development of microwave technologies for the oil and gas extraction complex," in *Proc. 4th Int. Conf. Antenna Theory Techn.*, 2003, pp. 101–104.
[9] S. Y. Chen, W. C. Chew, V. R. N. Santos, K. Sainath, and F. L. Teixeira, "Electromagnetic subsurface remote sensing," in *Wiley Encyclopedia of Electrical and Electronics Engineering*. New York, NY, USA: Wiley, 2016.
[10] R. S. Kallweit and L. C. Wood, "The limits of resolution of zero-phase wavelets," *Geophysics*, vol. 47, pp. 1035–1046, Jul. 1982.
[11] P. D. L. Beasley, "Advances in millimetre wave FMCW radar," in *Proc. MRRS Symp.*, Kiev, Ukraine, 2008, pp. 246–249.
[12] *FMCW Radar Sensors Application Notes*, SiversIMA, Stockholm, Sweden, 2011.
[13] J. H. Bradford and H. Marshall, "Estimating complex dielectric permittivity of soils from spectral ratio analysis of swept frequency (FMCW) ground-penetrating radar data (invited)," presented at the Amer. Geophys. Union, Fall Meeting, 2010.
[14] J. Blanche, D. Flynn, H. Lewis, G. Couples, and R. Cheung, "Analysis of geomaterials using frequency modulated continuous waves," presented at the 13th Int. Conf. Condition Monit. Machinery Failure Prevention Technol., Paris, France, 2016.
[15] J. Blanche, D. Flynn, H. Lewis, G. Couples, and R. Cheung, "Analysis of geomaterials using frequency modulated continuous wave radar in the X-band," presented at the IEEE 26th Int. Symp. Ind. Electron. (ISIE), Edinburgh, U.K., Jun. 2017.
[16] J. Blanche, D. Flynn, H. Lewis, G. Couples, and R. Cheung, "Analysis of geomaterials using frequency modulated continuous wave radar in the X-band," presented at the 1st World Congr. Condition Monit., London, U.K.: ILEC, 2017.
[17] A. G. Stove, "Issues with consistent generic representations of a radar," in *Proc. Int. Conf. Radar*, Adelaide, SA, Australia, 2008, pp. 1–4.
[18] J. Schön, *Physical Properties of Rocks: A Workbook*, vol. 8. Oxford, U.K.: Elsevier, 2011.
[19] P. Kaminski, K. Staszek, K. Wincza, and S. Gruszczynski, "K-band FMCW radar module with interferometic capability for industrial applications," presented at the 15th Int. Radar Symp. (IRS), 2014.
[20] R. Yadav, P. K. Dahiya, and R. Mishra, "A high performance 76.5 GHz FMCW RADAR for advanced driving assistance system," in *Proc. 3rd Int. Conf. Signal Process. Integr. Netw. (SPIN)*, Noida, India, 2016, pp. 383–388.
[21] G. Vinci *et al.*, "24 GHz six-port medical radar for contactless respiration detection and heartbeat monitoring," in *Proc. 9th Eur. Radar Conf.*, Amsterdam, The Netherlands, 2012, pp. 75–78.
[22] Ø. Aardal, Y. Paichard, S. Brovoll, T. Berger, T. S. Lande, and S.-E. Hamran, "Physical working principles of medical radar," *IEEE Trans. Biomed. Eng.*, vol. 60, no. 4, pp. 1142–1149, Apr. 2013.
[23] C. Li, V. M. Lubecke, O. Boric-Lubecke, and J. Lin, "A review on recent advances in Doppler radar sensors for noncontact healthcare monitoring," *IEEE Trans. Microw. Theory Techn.*, vol. 61, no. 5, pp. 2046–2060, May 2013.
[24] D. S. Herd, "Microwave based monitoring system for corrosion under insulation," Ph.D. dissertation, Inst. Signals, Sensors Syst., School Eng. Phys. Sci., Heriot-Watt University, Scotland, U.K., 2016.
[25] R. E. Jones, "Use of microwaves for the detection of corrosion under insulation," Ph.D. dissertation, Dept. Mech. Eng., Imperial College London, London, U.K., 2012.
[26] R. E. Jones, F. Simonetti, M. J. S. Lowe, and I. P. Bradley, "Use of microwaves for the detection of water as a cause of corrosion under insulation," *J. Nondestruct. Eval.*, vol. 31, no. 1, pp. 65–76, 2011.
[27] H. Gubler and M. Hiller, "The use of microwave FMCW radar in snow and avalanche research," *Cold Regions Sci. Technol.*, vol. 9, pp. 109–119, Jul. 1984.
[28] J. Holmgren, M. Sturm, N. E. Yankielun, and G. Koh, "Extensive measurements of snow depth using FM-CW radar," *Cold Regions Sci. Technol.*, vol. 27, pp. 17–30, Feb. 1998.
[29] H.-P. Marshall, M. Schneebeli, and G. Koh, "Snow stratigraphy measurements with high-frequency FMCW radar: Comparison with snow micropenetrometer," *Cold Regions Sci. Technol.*, vol. 47, pp. 108–117, Jan. 2007.
[30] H.-P. Marshall and G. Koh, "FMCW radars for snow research," *Cold Regions Sci. Technol.*, vol. 52, no. 2, pp. 118–131, 2008.
[31] N. Galin *et al.*, "2–8 GHz FMCW radar for estimating snow depth on antarctic sea ice," in *Proc. Int. Conf. Radar*, Adelaide, SA, Australia, 2008, pp. 276–281.
[32] N. Galin, A. Worby, T. Markus, C. Leuschen, and P. Gogineni, "Validation of airborne FMCW radar measurements of snow thickness over sea ice in Antarctica," *IEEE Trans. Geosci. Remote Sens.*, vol. 50, no. 1, pp. 3–12, Jan. 2012.
[33] J.-B. Yan *et al.*, "Ultrawideband FMCW radar for airborne measurements of snow over sea ice and land," *IEEE Trans. Geosci. Remote Sens.*, vol. 55, no. 2, pp. 834–843, Feb. 2017.
[34] S. Ayhan *et al.*, "Millimeter-wave radar sensor for snow height measurements," *IEEE Trans. Geosci. Remote Sens.*, vol. 55, no. 2, pp. 854–861, Feb. 2017.
[35] R. Kwok *et al.*, "Airborne surveys of snow depth over arctic sea ice," *J. Geophys. Res.*, vol. 116, p. C11018, Nov. 2011.
[36] B. Panzer *et al.*, "An ultra-wideband, microwave radar for measuring snow thickness on sea ice and mapping near-surface internal layers in polar firn," *J. Glaciol.*, vol. 59, no. 214, pp. 244–254, 2013.
[37] B. U. Felderhof, "Bounds for the effective dielectric constant of disordered two-phase materials," *J. Phys. C, Solid State Phys.*, vol. 15, no. 8, pp. 1731–1739, 1982.
[38] A. Robert, "Dielectric permittivity of concrete between 50 MHz and 1 GHz and GPR measurements for building materials evaluation," *J. Appl. Geophys.*, vol. 40, pp. 89–94, Oct. 1998.
[39] R. P. Wharton, R. N. Rau, and D. L. Best, "Electromagnetic propagation logging: Advances in technique and interpretation," presented at the SPE Annu. Tech. Conf. Exhib., 1980.
[40] P. F. Kerr, *Optical Mineralogy*, 3rd ed. New York, NY, USA: McGraw Hill, 1959.
[41] M. E. Tucker, *Sedimentary Rocks in the Field: A Practical Guide*, 4th ed. Chichester, U.K.: Wiley, 2011.
[42] (Sep. 11, 2017). *Stancliffe Stone Darney Sandstone Technical Data Sheet*. [Online]. Available: http://www.stancliffe.com/assets/Stancliffe/ProductInformation/PDFs/StoneTypes/Stancliffe-Stone-Darney-Sandstone.pdf
[43] (Sep. 11, 2017). *Stancliffe Stone Plumpton Red Lazonby Sandstone Technical Data Sheet*. [Online]. Available: http://www.stancliffe.com/assets/Stancliffe/ProductInformation/PDFs/StoneTypes/Stancliffe-Stone-Plumpton-Red-Lazonby-Sandstone.pdf
[44] (Sep. 11, 2017). *Stancliffe Stone Locharbriggs Red Sandstone Technical Data Sheet*. [Online]. Available: http://www.stancliffe.com/assets/Stancliffe/ProductInformation/PDFs/StoneTypes/Stancliffe-Stone-Locharbriggs-Red-Sandstone.pdf
[45] (Sep. 11, 2017). *Stancliffe Stone Red St Bees Sandstone Technical Data Sheet*. [Online]. Available: http://www.stancliffe.com/assets/Stancliffe/ProductInformation/PDFs/StoneTypes/Stancliffe-Stone-Red-St-Bees-Sandstone.pdf
[46] W. J. Duffin, "Electromagnetic waves," in *Electricity and Magnetism*, 4th ed. Berkshire, U.K.: McGraw-Hill, 1990, pp. 366–368.
[47] F. T. Ulaby, T. H. Bengal, M. C. Dobson, J. R. East, J. B. Garvin, and D. L. Evans, "Microwave dielectric properties of dry rocks," *IEEE Trans. Geosci. Remote Sens.*, vol. 28, no. 3, pp. 325–336, May 1990.

JAMIE BLANCHE received the B.Sc. degree (Hons.) in physics with environmental science and the M.Sc. degree in petroleum geoscience from Heriot-Watt University in 2003 and 2014, respectively, attaining upstream petroleum industry experience prior to achieving his M.Sc. degree. He is currently engaged in Ph.D. research at Heriot Watt University, working on the fusion of internal and external sensing methodologies for laboratory-based geomechanical monitoring. In 2015, he joined the Smart Systems Group, Heriot-Watt University. His research interest is the novel use of radar sensing and elastico-mechano-luminescence (EML) to determine *in situ* flow characteristics within deformed rocks and "pseudorock" analogues, serving as a platform for preliminary work in real-time sensing within an extreme environment and a departure from current practices of post-failure analysis. His work aims to inform improved hydrocarbon extraction strategies, in addition to the augmentation of current geomechanical imaging techniques.

DAVID FLYNN received the B.Eng. degree (Hons)–1st Class in electrical and electronic engineering, the M.Sc. degree (Hons.) in microsystems, and the Ph.D. degree in microscale magnetic components from Heriot-Watt University, Edinburgh, U.K., in 2002, 2003, and 2007, respectively. He is currently a Professor of electrical and electronic engineering with Heriot-Watt University. He is the founder of the Smart Systems Group (SSG) at Heriot-Watt University. He is also a Faculty Leader in smart systems integration, electrical engineering, and energy systems. The activities of the SSG involve multidisciplinary expertise in sensor technologies, data analysis, and systems engineering, to create predictive and prescriptive analysis of systems. He is an Institute of Engineering and Technology (IET) Scholar and also a recipient of the IET Leslie H Paddle Prize.

HELEN LEWIS received the B.Sc. and M.Sc. degrees in structural geology and rock mechanics from Imperial College, University of London, and the Ph.D. degree from Glasgow University, where she concurrently held a research position in flow in deforming fractured media. Before the completion of her Ph.D. degree at Glasgow, she held a position at the Centre for Tectonophyics, Texas A&M University, and then spent 10 years in the U.S. Oil and Gas Industry. She is currently an Associate Professor with the Institute of Petroleum Engineering, Heriot-Watt University, Edinburgh. Her research focuses on natural and laboratory-deformed rock systems covering topics, such as structural geology and geomechanics, full field rock mechanics lab testing, neutron- and X-ray tomographic techniques to detect deformation-flow responses and the development, and use of sensor systems within deforming rocks. She has held multiple funded projects across these topics, currently in X-ray and neutron tomography, sensor systems, and limestone rock system deformation.

GARY D. COUPLES received the B.S. degree from the Texas A&M University in 1974, the M.A. degree from Rice University in 1977, and the Ph.D. degree from Texas A&M University in 1986. He was with Cities Service (Tulsa) and Amoco (Denver), and ran a consultancy, before joining the academic world in 1989, first at Glasgow University (Scotland), before moving to Heriot-Watt University, Edinburgh, U.K., in 1998. He is currently a Professor of geomechanics with the Institute of Petroleum Engineering, Heriot-Watt University, where he is involved in the engineering-geology interface. He is also a faculty of three master's courses at Heriot-Watt University (lecturing to engineers and geoscientists), and also a geomechanics master programme at the Université Joseph Fourier, Grenoble, France. His research links geomechanical effects to their consequences. He was an SPE Distinguished Lecturer from 2013 to 2014, speaking on geomechanical issues in fractured reservoirs. He uses textural analysis and digital rocks in an effort to understand how rock properties are controlled by their depositional, diagenetic, and deformation histories.

JIM BUCKMAN is currently a Research Fellow with the Institute of Petroleum Engineering, Heriot-Watt University, where he manages the scanning electron microscope (SEM) facility. He has a background in geological sciences and undertakes a range of SEM-based research into mudrocks, sandstones, carbonates, biological materials, wettability, and develops microscope techniques involving automation and analysis.

CHRIS BAILEY (A'00–M'03–SM'05) received the MBA degree in technology management from the Open University, Milton Keynes, U.K., in 1996, and the Ph.D. degree in computational modeling from Thames Polytechnic, London, U.K., in 1988. He was a Research Fellow of materials engineering with Carnegie Mellon University, Pittsburgh, PA, USA, for three years. He is currently a Professor of the Computational Mechanics and Reliability Group, University of Greenwich. His current research interests include the development of virtual prototyping tools based on multiphysics modeling and numerical optimization. He is a Committee Member with the International Microelectronics and Packaging Society and the Innovative Electronics Manufacturing Research Centre, U.K.

TIMOTHY TILFORD was born in London, U.K., in 1974. He received the bachelor's degree in aeronautical engineering from Queen Mary College, University of London, U.K., in 1998, the master's degree in computational fluid dynamics from the University of Greenwich, U.K., in 1999, and the Ph.D. degree in computational mechanics from the University of Greenwich in 2013. Since 2002, he has been a Research Fellow and subsequently a Senior Lecturer at the University of Greenwich. His primary research interests are in numerical analysis of multiphysics/multi-scale problems and high performance parallel computing. He is a Fellow of the Institute of Mathematics and its Applications, a Chartered Mathematician, and a Chartered Scientist.